Dyes and Pigments 147 (2017) 113–119

Contents lists available at ScienceDirect

Dyes and Pigments

journal homepage: www.elsevier.com/locate/dyepig

Tetrathiafulvalene derivative as a new hole-transporting material for highly efficient perovskite solar cell

Qiushan Chen [a, b], Xiaodong Li [a], Tonggang Jiu [a, **], Sushuang Ma [a], Jiangsheng Li [a], Xunwen Xiao [c], Wenjun Zhang [a, *]

[a] Key Laboratory of Graphene Technologies and Applications of Zhejiang Province, Institute of Materials Technology and Engineering, Chinese Academy of Sciences, Ningbo 315201, China
[b] College of Material Science and Chemical Engineering, Ningbo University, Ningbo 315211, China
[c] School of Materials and Chemical Engineering, Ningbo University of Technology, 315211, China

ARTICLE INFO

Article history:
Received 31 May 2017
Received in revised form
19 July 2017
Accepted 6 August 2017
Available online 8 August 2017

Keywords:
Perovskite solar cells
Hole-transporting material
Tetrathiafulvalene derivative
Carboxylic acid
Energy level

ABSTRACT

Hole-transporting materials play an important role in perovskite solar cells. In this study, we introduced a novel hole-transporting material without p-type dopant, a tetrathiafulvalene derivative anchored with eight carboxyl groups (TTA) into inverted structure perovskite solar cells. The devices with TTA as hole-transporting layer showed high power conversion efficiency of 16.7%, which was 44.5% improvement compared with the reference devices without hole-transporting layer. The performance improvement was ascribed to three factors: 1) the better match of energy level between ITO and perovskite layer; 2) enhanced hole extraction at anode interface; 3) improved perovskite morphology.

1. Introduction

Organic-inorganic hybrid perovskite solar cells (PSCs) have attracted worldwide attentions in the past few years due to their intriguing properties, such as large absorption coefficient, low excitation energy, long electron-hole diffusion length, easy fabrication and low cost [1–10]. The power conversion efficiency (PCE) of perovskite solar cells has rocketed over 22% from initial 3.8% in the last few years [11–14]. Throughout the development of PSCs, hole-transporting materials (HTMs) play an important role in rapid development of PSCs. The commonly used HTM in PSCs like 2,2′,7,7′-tetrakis-(*N*,*N*-di-*p*-methoxyphenylamine)-9,9′-spirobifluorene (spiro-OMeTAD) [15,16], poly-(triarylamine) (PTAA) [17] and so on, need *p*-doping to increase its conductivity [18,19], ascribe to the sp^3 hybridization of the nitrogen atom leading to large intermolecular distances in their pristine and undoped form [20,21]. Although a tiny doping can marvelously increase fill factor (FF) and short-circuit current density (J_{sc}) by modulating conductivity, the p-type doping strategy for HTM requires strict optimization such as the doping concentrations and time [17,22], thus making the manufacture processing of the PSCs complicated and time-consuming for actual application. So it is important to develop novel and undoped HTM for cost-effective production of high-performance PSCs.

Tetrathiafulvalene and its derivatives have been extensively investigated as electron-donating unit in molecular conductors due to strong intermolecular π-π stacking [23,24]. They have presented wide applications in many areas of materials chemistry [25–29], while the employment of tetrathiafulvalene and its derivatives in PSCs was rare [30,31]. Jian et al. introduced a tetrathiafulvalene derivative TTF-1 into PSCs with typical structure, without the use of p-type dopants. The TTF-1 PSCs exhibited a comparable efficiency to the spiro-OMeTAD PSCs and better humidity stability. However, the efficiency is moderate and the typical structure PSCs needs a TiO_2 layer with high temperature treatment. In this study, we employed a tetrathiafulvalene derivative 5,5′,5″,5‴-(tetrathiafulvalene-2,3,6,7-tetrayl)tetraisophthalic acid (TTA) as an HTM without p-type dopant and achieved highly efficient inverted PSCs through low-temperature solution-processing. By the introduction

* Corresponding author.
** Corresponding author.
E-mail addresses: jiutg@qibebt.ac.cn (T. Jiu), zhangwenjun@nimte.ac.cn (W. Zhang).

http://dx.doi.org/10.1016/j.dyepig.2017.08.007
0143-7208/

of hydrophilic carboxyl groups into tetrathiafulvalene, we successfully modify the wetting property of tetrathiafulvalene and the inverted PSCs were fabricated. After introducing TTA HTM, the perovskite morphology can improved, leading to higher device efficiency and device lifetime. Importantly, notorious device hysteresis was reduced in PSCs with TTA as HTM. All these results indicated that TTA was a novel, efficient HTM in PSCs, which may enrich the material system of HTM in PSCs, further promoting the development of un-doped HTM.

2. Experimental section

2.1. Materials

CH_3NH_3I and PbI_2 were purchased from Xi'an, China Polymer Light Technology Corp. (6,6)-Phenyl-C61-butyric acid methyl ester ($PC_{61}BM$) and C_{60} were purchased from American Dye Source. 2,9-Dimethyl-4,7-diphenyl-1,10-phenanthroline (BCP) was purchased from J&K Scientific Ltd. Poly(3,4-ethylenedioxythiophene): polystyrene sulfonic acid (PEDOT:PSS) (Clevious P VP AI 4083) was purchased from H. C. Stark company. TTA was synthesized according to an unpublished work.

2.2. Device fabrication and characterization

ITO glasses were cleaned through sequential sonication in detergent, deionized water, acetone, and isopropyl alcohol for 20 min. Then ITO glasses were dried using N_2 flow and moved to Plasma chamber for 10 min. After that, TTA solution in anhydrous N,N−dimethylformamide (DMF, Aldrich) (10 mg/mL) was spin-coated on ITO glasses at 4000 rpm for 60 s to form approximately 20 nm thin films and then annealed at 140 °C for 10 min in air. Then the substrates were transferred into glovebox (filled with N_2). The precursor solution of perovskite was prepared with CH_3NH_3I and PbI_2 at a mole ratio of 1:1 with the concentration at 1.4 M in 1 mL mixture of anhydrous DMF and anhydrous dimethylsulfoxide (DMSO, Aldrich) (8:2 by volume). Then the perovskite precursor solution was spin-coated at 4800 rpm for 30 s. During the spin-coating process, 400 μL of anhydrous chlorobenzene (CB, Aldrich) was slowly dripped on the rotating substrate to obtain a highly uniform and approximately 400 nm perovskite film. Then the substrate was annealed at 60 °C for 1 min and 80 °C for 2 min. Sequentially, $PC_{61}BM$ solution in CB (20 mg/mL) was spin-coated on $CH_3NH_3PbI_3$ layer at 2000 rpm for 1 min to form approximately 40 nm electron-transporting layer. Finally, the devices were transferred to vacuum chamber (10^{-6} mbar), 20 nm C_{60}, 8 nm BCP and 100 nm Ag were evaporated respectively. The area of the device was defined to be 6 mm^2 with shadow mask. Current density-voltage (*J-V*) measurements were conducted using Keithley 2400 sourcemeter controlled by computer. All the PSCs were measured under Newport 6279 NS solar simulator (450 W) with 100 mW/cm^2. The EQE measurements were conducted through the Newport quantum efficiency measurement system (ORIEL IQE 200TM). The film thickness was measured using a surface profiler (Veeco, Dektak 150). The light intensity at each wavelength was calibrated by one standard Si/Ge solar cell. Ultraviolet photoelectron spectroscopy (UPS) measurements were conducted using Shimadzu Spectrometer (AXIS ULTRA DLD) with a He (21.2 eV) discharge lamp to measure energy level of the bare ITO and the TTA. X-ray diffraction (XRD) measurements were performed using a D8 Advance (Bruker AXS) with a Cu Ka (l ¼ 1.54 Å) radiation source to measure crystal structure of $CH_3NH_3PbI_3$ based on different substrates. Scanning electron microscopy (SEM, S-4800, Hitachi) operated at an acceleration voltage of 8 kV to observe surface morphology of $CH_3NH_3PbI_3$ layer and atomic force microscopy (AFM, Dimension 3100 V, Veeco, tapping mode) measurements were used to observe the surface morphology of the bare ITO and the TTA films. The photoluminescence (PL) measurements of perovskite films were conducted using Horiba (FL3-111) at ambient atmosphere. The films were photoexcited using a 600 nm monochromatic light and

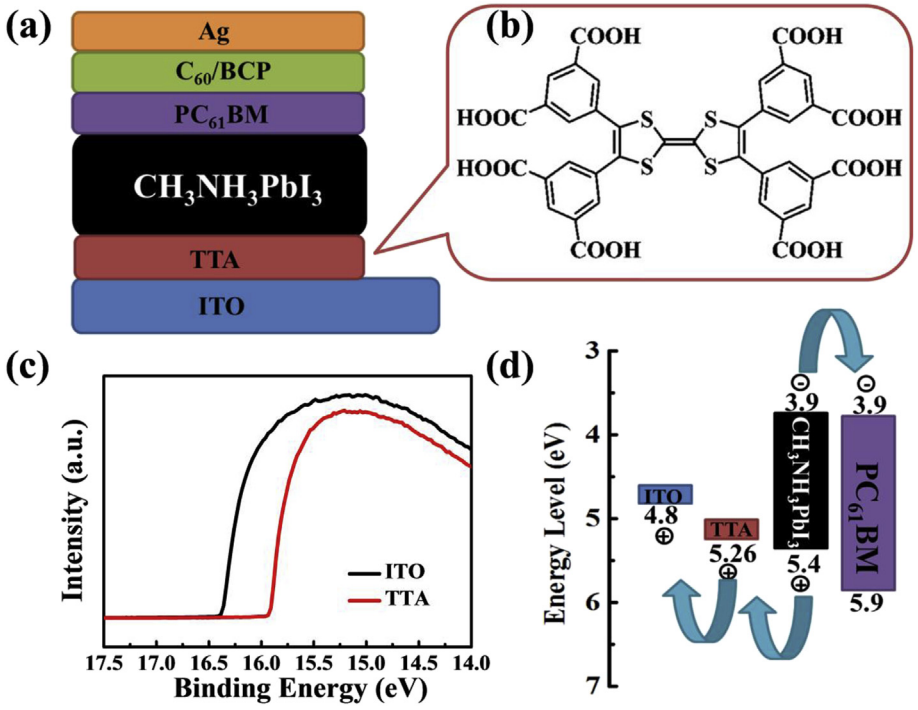

Fig. 1. (a) The device structure of the PSCs with TTA as HTM and Ag layer as the top cathode. (b) Chemical structures of TTA. (c) UPS of ITO glass and the TTA coated ITO glass. (d) Energy-level diagram of the PSCs, exhibiting the collecting process of photo generated charge carriers.

detected the PL at 780 nm. The time-resolved photoluminescence (TRPL) measurements were obtained from a single photon counting spectrometer on Edinburgh Instruments (FLS920) with a Picosecond Pulsed UVLASTER (LASTER337) as the excitation light source.

3. Results and discussion

Fig. 1(a) illustrates devices architecture where the TTA film is used as the HTM, $PC_{61}BM$ and C_{60} as the electron-transporting materials, BCP as the hole-blocking layer and Ag as the top cathode. $CH_3NH_3PbI_3$ was deposited using a fast crystallization method, which was first developed by Xiao et al. [32] The molecular structure of TTA is shown in Fig. 1(b). The work function (WF) of the ITO and ITO/TTA was measured using UPS measurement as shown in Fig. 1(c). The WF of the bare ITO is4.80 eV, while its WF increases to 5.26 eV after deposition of TTA, which was much close to the valence band of perovskite (5.40 eV). Fig. 1(d) shows the energy-level alignment of our PSCs. The decrease of mismatch would reduce the energy loss at ITO/perovskite interface, thus facilitating more efficient hole collection and increasing the built-in potential and corresponding performance of inverted PSCs [33,34].

Fig. 2(a) presents the *J-V* curves of the PSCs based on different substrates. The detailed *J-V* parameters are summarized in Table S1. For devices without TTA, the performance was poor with a PCE of 11.57%, a J_{sc} of 17.4 mA cm^{-2}, an open-circuit voltage (V_{oc}) of 0.95 V and a FF of 0.70. When introducing TTA, the device performance can be greatly improved. The *J-V* curves of PSCs are shown in Fig S1 as a function of the TTA concentration. The optimal PCE appeared when the TTA concentration was 10 mg/mL and the best device based on TTA exhibited a J_{sc} of 20.4 mA cm^{-2}, a V_{oc} of 1.04 V, a FF of 0.78 and a PCE of 16.7%. One reason for the improvement of all photovoltaic parameters in the TTA based devices was suitable energy level gradient, thus reducing the energy loss at ITO/perovskite interface, leading to effective hole collection and extraction from perovskite light absorber to anode. Fig. 2(b) displays the incident photon-to-current conversion efficiency (IPCE) and the integrated product of the IPCE curves with the AM 1.5G photon flux. The integral J_{sc} value from the IPCE for the devices with TTA inserting is19.7 mA cm^{-2} and the reference is 16.6 mA cm^{-2} which are comparable to the direct *J-V* measurements. Fig S2 displays the J_{sc}, V_{oc}, FF and PCE distribution histograms of devices based on different substrates with the statistics. It appeared that all the key parameters of the devices with the TTA inserting had fairly narrow distribution, indicating that the PSCs with the TTA HTM presented very good reproducibility. For another reference, we also fabricated PSCs with PEDOT:PSS which was diluted 10 times with H_2O as HTM. The PEDOT:PSS device displayed inferior performance for as-yet-unknown reasons, although the same processing conditions to the TTA devices (Fig. 2(a)). And the *J-V* curves of the PEDOT:PSS PSCs with different scanning direction are also shown in Fig S3.

The anomalous photocurrent hysteresis was shown to be a major issue in accurately characterizing device efficiency which was observed in many PSCs. It was reported that the hysteresis was originated from electromigration of ions, ferroelectric properties and the traps in the perovskite films [35,36]. By optimizing interfaces, some group successfully fabricated planar heterojunction PSCs by interface modification with bare hysteresis [37–39]. Therefore, *J-V* curves of these devices with different scanning direction and scanning rates were tested in our study. Fig. 2(c) presents the *J-V* curves of devices with TTA under different scan rates, showing little difference. The results indicated that the devices with TTA can effectively decrease charge accumulation due to the high hole mobility and support suitable energy level gradient. So insertion of TTA resulted in effectively decreasing hysteresis of the inverted PSCs. The *J-V* curves of TTA PSCs with different scanning direction are also shown in Fig S4 and corresponding photovoltaic parameters are presented in Table S1. There is also little difference (about 5%) between the forward scan and the reverse scan. The steady state photocurrent representing the actual power output

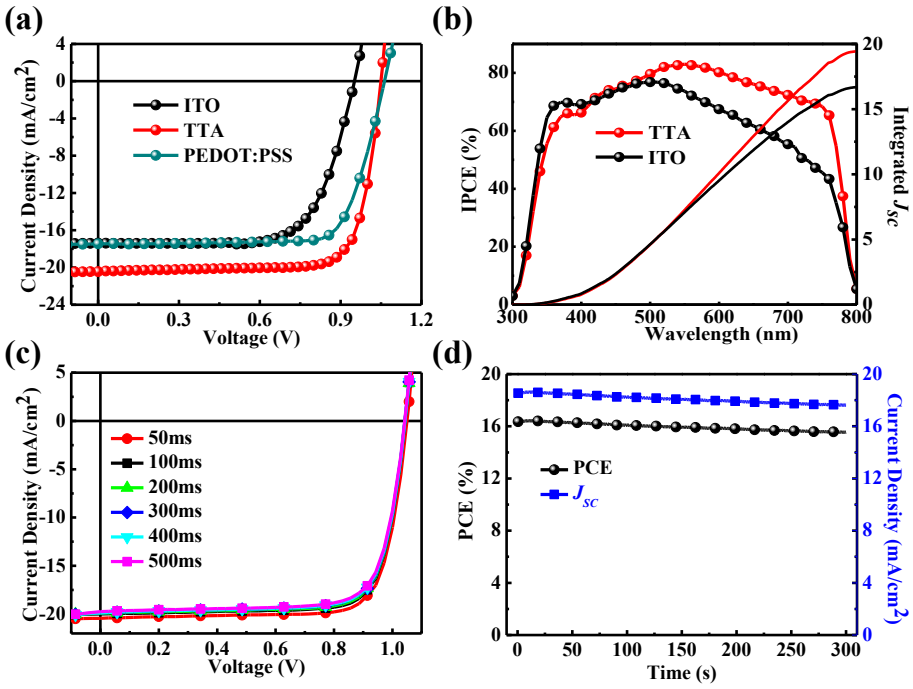

Fig. 2. (a) *J-V* characteristic curves of PSCs obtained from forward bias to short circuit (FB-SC). (PEDOT:PSS is diluted 10 times with H_2O). (b) IPCE of PSCs based on different substrates. (c) *J-V* characteristic curves of the PSCs based on TTA measured with different delay between measurement points (d) Steady-state efficiency and photocurrent density of the PSCs based on TTA as a function of time applied at a forward bias of 0.885 V.

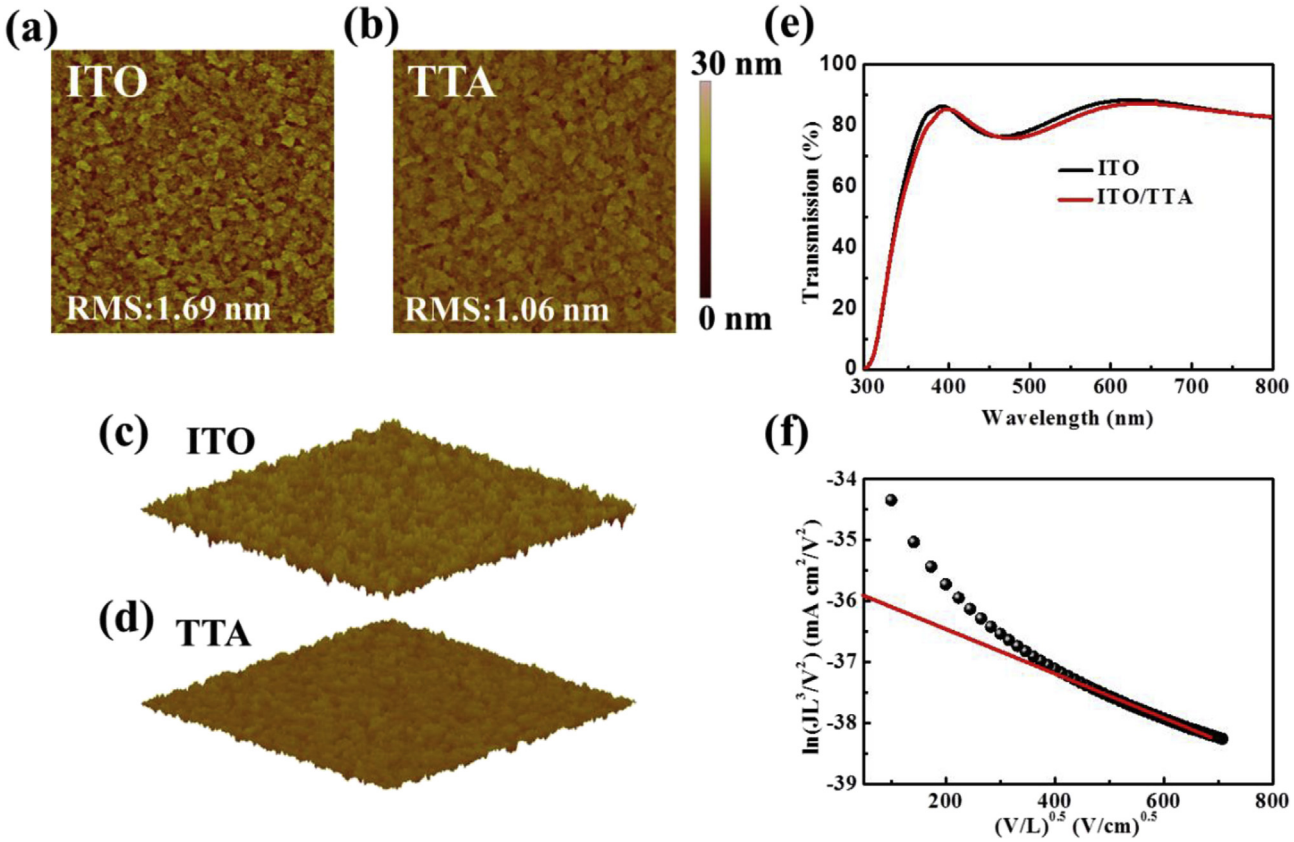

Fig. 3. (a) AFM height images of the bare ITO films and (b) the ITO/TTA films with a scan size of 5 × 5 μm. (c) Corresponding 3D images of the bare ITO glasses and (d) the ITO/TTA films. (e) Transmittance spectrum of the bare ITO films and the ITO/TTA films. (f) Current-voltage data from the devices of ITO/PEDOT:PSS/TTA/MoO_3/Al, plotted in the format $\ln(JL^3/V^2)$ versus $(V/L)^{0.5}$, where J is the current density and L is the thickness of the TTA layer. The lines are the fit to the respective experimental points.

was used to characterize accurate device efficiency. In order to verify the enhanced efficiency, we recorded the photocurrent of the devices with TTA held at their maximum power point voltage (0.885 V for TTA modified device) under AM 1.5G 100 mW/cm^2 simulated solar light. As shown in Fig. 2(d), the steady-state current and PCE are nearly the same as that measured from the photocurrent measurement. This suggested that the improvement of PCE for the devices with TTA was reliable.

AFM was measured and the height images of the bare ITO glasses and the ITO/TTA films are presented in Fig. 3(a and b). When the TTA solution was spin-coated onto the ITO substrate, TTA formed a continuous film with uniform coverage. The root-mean-square (RMS) roughness decreased to 1.06 nm from 1.69 nm for the bare ITO substrate. Fig. 3(e) exhibits the optical transmittance spectrum of the bare ITO and the ITO/TTA film. The transmittance of TTA coated ITO is around 80% in the whole range from 380 nm to 800 nm, indicating that the ITO/TTA film would allow nearly the same photon flux to reach perovskite film.

To explore the origins of the increasing J_{sc}, the hole mobility was approximated using space charge limited current measurement in which device structure was ITO/PEDOT:PSS/TTA/MoO_3/Ag, the detailed process is shown in the Supporting Information. As shown in Fig. 3(f), the result was plotted as $\ln(JL^3/V^2)$ versus $(V/L)^{0.5}$ by fitting to the Mott-Gurney law [40]. The hole mobility of TTA was calculated from the intercept of the corresponding lines on the axis of $\ln(JL^3/V^2)$. It was easy to obtain that hole mobility of the TTA based hole-only device was 9.68 × 10^{-4} cm^2 V^{-1} s^{-1} which was comparable to the high hole mobility of the well-known dopant enhanced spiro-OMeTAD HTM [41]. The high hole mobility of TTA contributed significantly to the high J_{sc} and FF for the PSCs.

In order to understand the influence of different substrates on the crystallization for perovskite films, the resultant films produced by different substrates were characterized by XRD measurements. XRD measurements on our perovskite thin films show typical $CH_3NH_3PbI_3$ (110), (220) and (310) peak at 14.2°, 28.5° and 32.0°, respectively (Fig. 4(a)) [37]. To further investigate crystal growth of perovskite deposited on different substrates, SEM was employed to investigate the morphology change due to the TTA inserting which influenced the growth of perovskite film. Fig. 4(b and c) shows the surface morphology of perovskite deposited on the bare ITO glasses and the TTA films, respectively. It was obvious that there was a striking contrast between the ITO/$CH_3NH_3PbI_3$ film and the TTA/$CH_3NH_3PbI_3$ film. There were lots of cracks in the ITO/$CH_3NH_3PbI_3$ film, while none of them could be seen in the TTA/$CH_3NH_3PbI_3$ film. Meanwhile, the crystal grain of perovskite film based on the TTA substrates was more uniform than the crystal grain of perovskite film on top of ITO substrates, leading to improved FF in the photovoltaic performance. So the high quality of $CH_3NH_3PbI_3$ film based on the TTA anode interfacial layer would also prevent the potentially direct contact of electrodes, thus inhibiting the leakage current and further improving the J_{sc} and FF. On the one hand, as upper mentioned TTA formed a continuous film with uniform coverage, this would contribute to the high-quality $CH_3NH_3PbI_3$ on the TTA. On the other hand, interface energy of substrates may also affect the perovskite film morphology on top [42]. Indeed, the TTA is more hydrophobic than ITO glasses (Fig. S5). In a word, the TTA film was a suitable substrate for growth of the higher quality perovskite light absorber film.

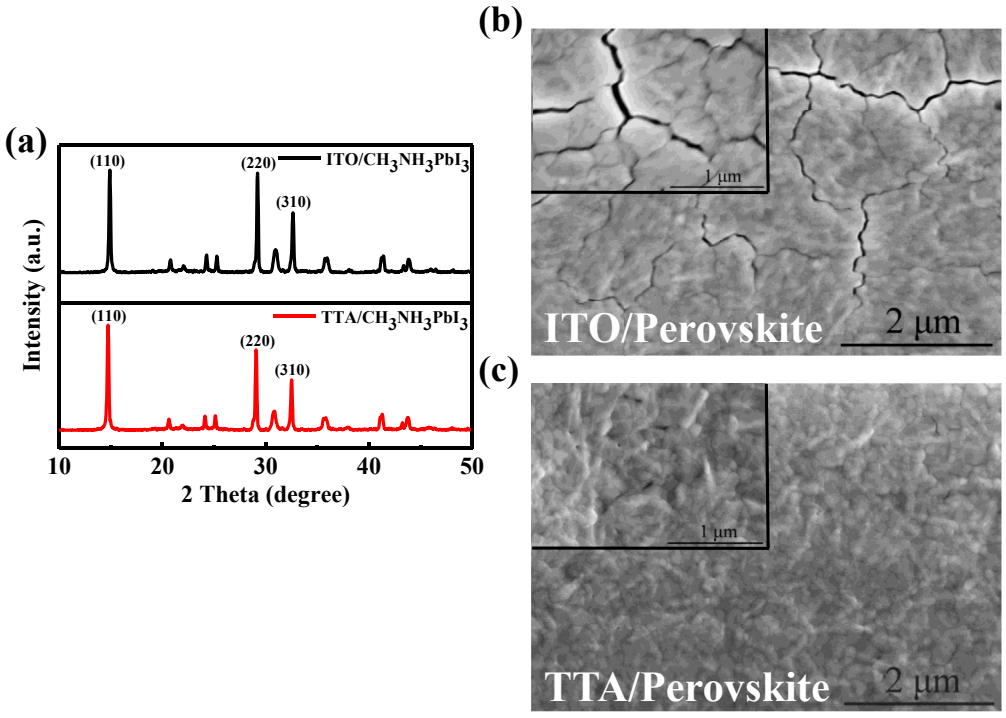

Fig. 4. (a) The XRD of the $CH_3NH_3PbI_3$ films on the bare ITO substrates and the ITO/TTA substrates. Top view SEM images of (b) ITO/$CH_3NH_3PbI_3$ thin film, (c) TTA/$CH_3NH_3PbI_3$ thin film. Scale bar is 2 μm. (iner bar is 1 μm).

In order to investigate whether TTA can efficiently extract photo-generated carriers from the perovskite film, PL and TRPL were carried out for $CH_3NH_3PbI_3$ films on different substrates. Fig. 5(a) shows the steady state PL spectra of the ITO/$CH_3NH_3PbI_3$ and the TTA/$CH_3NH_3PbI_3$ under the same experimental condition. Compared to the ITO/$CH_3NH_3PbI_3$ sample, the PL intensity of TTA/$CH_3NH_3PbI_3$ was significantly quenched, further demonstrating that TTA was effective in hole extraction due to the high hole mobility and suitable energy level. Fig. 5(b) shows the TRPL for ITO/$CH_3NH_3PbI_3$ film and TTA/$CH_3NH_3PbI_3$ film. The lifetime of carriers were acquired by fitting the data with two exponential decay functions [43]. For ITO/$CH_3NH_3PbI_3$ film, the average PL lifetime was 10.6 ns, while the average PL lifetime for TTA/$CH_3NH_3PbI_3$ film was 6.8 ns. The decreased lifetime also indicated a faster hole-transfer process and more efficient hole extraction, leading to the high J_{sc} and FF.

Since device stability is also a key factor to the practical application, we also investigated the durability of the TTA PSCs in inert atmosphere and ambient conditions. As shown in Fig S5, the PSCs with and without TTA both exhibited a good stability in glove box. However, under ambient conditions at room temperature with a humidity of about 40%, the TTA devices also exhibited relatively slower degradation while the PCE of devices without TTA decayed quickly to almost zero after 9 days (Fig. 6). These results suggested that TTA was a promising solution-processed HTM for achieving air-stable and high-efficiency PSCs.

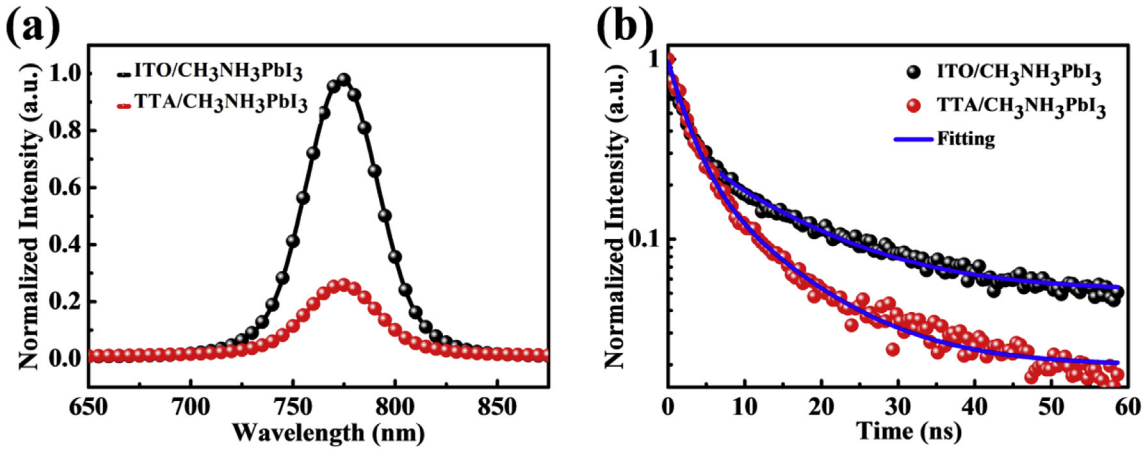

Fig. 5. (a) Steady state PL spectra of two films: ITO/$CH_3NH_3PbI_3$, TTA/$CH_3NH_3PbI_3$, The excitation light enters the sample from the glass substrate side with excitation at 600 nm, and PL spectra are collected. (b) TRPL spectra of $CH_3NH_3PbI_3$ films on the bare ITO substrates and the TTA substrates.

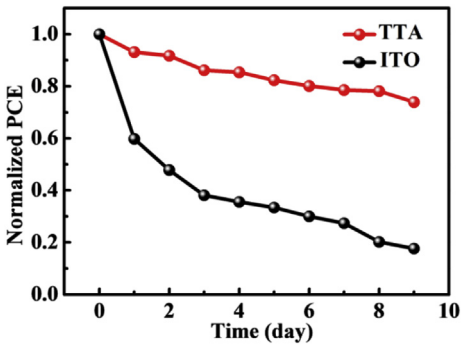

Fig. 6. (a) Efficiency variation of the devices based on different substrates. Unencapsulated devices were stored in air at room temperature with a humidity of about 40% were measured under illumination at AM 1.5 G.

4. Conclusion

In conclusion, we demonstrate that the employment of a carboxylic acid derivatives with tetrathiafulvalene core TTA at the ITO/$CH_3NH_3PbI_3$ interface is effective in improving the photovoltaic performance of PSCs and PCE of 16.7% could be obtained. The improved performance originates from well-aligned energy level and high hole mobility of TTA which is partly confirmed in the quenched photoluminescence intensity and shortened carrier lifetime. Additionally, SEM measurements indicate that the high quality perovskite films without cracks can be obtained on the TTA substrates which also leading to enhanced J_{sc} and FF. Therefore, our work prove that the TTA is a promising hole-transporting candidate without p-type dopant for PSCs application.

Acknowledgements

This work is financially supported by National Natural Science Foundation of China (51403222 and 21372136) and China Postdoctoral Science Foundation funded project (2017M610380).

Appendix A. Supplementary data

Supplementary data related to this article can be found at http://dx.doi.org/10.1016/j.dyepig.2017.08.007.

References

[1] Mei A, Li X, Liu L, Ku Z, Liu T, Rong Y, et al. A hole-conductor-ree, fully printable mesoscopic perovskite solar cell with high stability. Science 2014;345(6194):295–8.
[2] Xing G, Mathews N, Sun S, Lim SS, Lam YM, Grätzel M, et al. Long-range balanced electron-and hole-transport lengths in organic-inorganic $CH_3NH_3PbI_3$. Science 2013;342(6156):344–7.
[3] Dong Q, Fang Y, Shao Y, Mulligan P, Qiu J, Cao L, et al. Electron-hole diffusion lengths> 175 μm in solution-grown $CH_3NH_3PbI_3$ single crystals. Science 2015;347(6225):967–70.
[4] Kim H-S, Lee C-R, Im J-H, Lee K-B, Moehl T, Marchioro A, et al. Lead iodide perovskite sensitized all-solid-state submicron thin film mesoscopic solar cell with efficiency exceeding 9%. Sci Rep 2012;2. 591.
[5] Xiao Z, Bi C, Shao Y, Dong Q, Wang Q, Yuan Y, et al. Efficient, high yield perovskite photovoltaic devices grown by interdiffusion of solution-processed precursor stacking layers. Energy Environ Sci 2014;7(8):2619–23.
[6] Nie W, Tsai H, Asadpour R, Blancon J-C, Neukirch AJ, Gupta G, et al. High-efficiency solution-processed perovskite solar cells with millimeter-scale grains. Science 2015;347(6221):522–5.
[7] Zhu H, Fu Y, Meng F, Wu X, Gong Z, Ding Q, et al. Lead halide perovskite nanowire lasers with low lasing thresholds and high quality factors. Nat Mater 2015;14(6):636–42.
[8] Gao P, Grätzel M, Nazeeruddin MK. Organohalide lead perovskites for photovoltaic applications. Energy Environ Sci 2014;7(8):2448–63.
[9] Tan Z-K, Moghaddam RS, Lai ML, Docampo P, Higler R, Deschler F, et al. Bright light-emitting diodes based on organometal halide perovskite. Nat Nanotechnol 2014;9(9):687–92.
[10] You J, Hong Z, Yang YM, Chen Q, Cai M, Song T-B, et al. Low-temperature solution-processed perovskite solar cells with high efficiency and flexibility. ACS Nano 2014;8(2):1674–80.
[11] Kojima A, Teshima K, Shirai Y, Miyasaka T. Organometal halide perovskites as visible-light sensitizers for photovoltaic cells. J Am Chem Soc 2009;131(17):6050–1.
[12] Liu D, Kelly TL. Perovskite solar cells with a planar heterojunction structure prepared using room-temperature solution processing techniques. Nat Photonics 2014;8(2):133–8.
[13] Zhou H, Chen Q, Li G, Luo S, Song T-B, Duan H-S, et al. Interface engineering of highly efficient perovskite solar cells. Science 2014;345(6196):542–6.
[14] National Renewable Energy Laboratory (NREL), http://www.nrel.gov/ncpv/images/efficiency-chart.jpg [Accessed April 2016].
[15] Burschka J, Pellet N, Moon S-J, Humphry-Baker R, Gao P, Nazeeruddin MK, et al. Sequential deposition as a route to high-performance perovskite-sensitized solar cells. Nature 2013;499(7458):316–9.
[16] Wojciechowski K, Stranks SD, Abate A, Sadoughi G, Sadhanala A, Kopidakis N, et al. Heterojunction modification for highly efficient organic–inorganic perovskite solar cells. ACS Nano 2014;8(12):12701–9.
[17] Ryu S, Noh JH, Jeon NJ, Kim YC, Yang WS, Seo J, et al. Voltage output of efficient perovskite solar cells with high open-circuit voltage and fill factor. Energy Environ Sci 2014;7(8):2614–8.
[18] Abate A, Leijtens T, Pathak S, Teuscher J, Avolio R, Errico ME, et al. Lithium salts as "redox active" p-type dopants for organic semiconductors and their impact in solid-state dye-sensitized solar cells. Phys Chem Chem Phys 2013;15(7):2572–9.
[19] Noh JH, Jeon NJ, Choi YC, Nazeeruddin MK, Grätzel M, Seok SI. Nanostructured $TiO_2/CH_3NH_3PbI_3$ heterojunction solar cells employing spiro-OMeTAD/Co-complex as hole-transporting material. J Mater. Chem A 2013;1(38):11842–7.
[20] Leijtens T, Lim J, Teuscher J, Park T, Snaith HJ. Charge density dependent mobility of organic hole-transporters and mesoporous TiO_2 determined by transient mobility spectroscopy: implications to dye-sensitized and organic solar cells. Adv Mater 2013;25(23):3227–33.
[21] Burschka J, Dualeh A, Kessler F, Baranoff E, Cevey-Ha N-L, Yi C, et al. Tris (2-(1 H-pyrazol-1-yl) pyridine) cobalt (III) as p-type dopant for organic semiconductors and its application in highly efficient solid-state dye-sensitized solar cells. J Am Chem Soc 2011;133(45):18042–5.
[22] Wang Q, Bi C, Huang J. Doped hole transport layer for efficiency enhancement in planar heterojunction organolead trihalide perovskite solar cells. Nano Energy 2015;15:275–80.
[23] Nishida S, Morita Y, Fukui K, Sato K, Shiomi D, Takui T, et al. Spin transfer and Solvato-/Thermochromism Induced by intramolecular electron transfer in a purely organic open-shell system. Angew Chem Int Ed 2005;117(44):7443–6.
[24] Olaya AJ, Ge P, Gonthier JF, Pechy P, Corminboeuf C, Girault HH. Four-electron oxygen reduction by tetrathiafulvalene. J Am Chem Soc 2011;133(31):12115–23.
[25] Guldi DM, Gonzalez S, Martin N, Antón A, Garín J, Orduna J. Efficient charge separation in C60-Based dyads: triazolino [4′,5′:1,2][60] fullerenes. J Org Chem 2000;65(7):1978–83.
[26] Uchida K, Masuda G, Aoi Y, Nakayama K, Irie M. Synthesis of tetrathiafulvalene derivatives with photochromic diarylethene moieties. Chem Lett 1999;28(10):1071–2.
[27] Aksyuk V, Balakirev F, Boebinger G, Gammel P, Haddon R, Bishop D. Micromechanical "trampoline" magnetometers for use in large pulsed magnetic fields. Science 1998;280(5364):720–2.
[28] Palacio F, Miller JS. A dual-action material. Nature 2000;408:421–2.
[29] Wenger S, Bouit P-A, Chen Q, Teuscher J, Censo DD, Humphry-Baker R, et al. Efficient electron transfer and sensitizer regeneration in stable π-extended tetrathiafulvalene-sensitized solar cells. J Am Chem Soc 2010;132(14):5164–9.
[30] Amacher A, Yi C, Yang J, Bircher MP, Fu Y, Cascella M, et al. A quinoxaline-fused tetrathiafulvalene-based sensitizer for efficient dye-sensitized solar cells. Chem Commun 2014;50(49):6540–2.
[31] Liu J, Wu Y, Qin C, Yang X, Yasuda T, Islam A, et al. A dopant-free hole-transporting material for efficient and stable perovskite solar cells. Energy Environ Sci 2014;7(9):2963–7.
[32] Xiao M, Huang F, Huang W, Dkhissi Y, Zhu Y, Etheridge J, et al. A fast deposition-crystallization procedure for highly efficient lead iodide perovskite thin-film solar cells. Angew Chem Int Ed 2014;126(37):10056–61.
[33] Lim KG, Kim HB, Jeong J, Kim H, Kim JY, Lee TW. Boosting the power conversion efficiency of perovskite solar cells using self-organized polymeric hole extraction layers with high work function. Adv Mater 2014;26(37):6461–6.
[34] Li X, Liu X, Wang X, Zhao L, Jiu T, Fang J. Polyelectrolyte based hole-transporting materials for high performance solution processed planar perovskite solar cells. J Mater. Chem A 2015;3(29):15024–9.
[35] Snaith HJ, Abate A, Ball JM, Eperon GE, Leijtens T, Noel NK, et al. Anomalous hysteresis in perovskite solar cells. J Phys Chem Lett 2014;5(9):1511–5.
[36] Unger E, Hoke E, Bailie C, Nguyen W, Bowring A, Heumüller T, et al. Hysteresis and transient behavior in current–voltage measurements of hybrid-perovskite absorber solar cells. Energy Environ Sci 2014;7(11):3690–8.
[37] Yang D, Yang R, Ren X, Zhu X, Yang Z, Li C, et al. Hysteresis-suppressed high-efficiency flexible perovskite solar cells using solid-state ionic-liquids for effective electron transport. Adv Mater 2016;28(26):5206–13.
[38] Chen K, Hu Q, Liu T, Zhao L, Luo D, Wu J, et al. Charge-carrier balance for

highly efficient inverted planar heterojunction perovskite solar cells. Adv Mater 2016;28(48):10718–24.
[39] Kuang C, Tang G, Jiu T, Yang H, Liu H, Li B, et al. Highly efficient electron transport obtained by doping PCBM with graphdiyne in planar-heterojunction perovskite solar cells. Nano Lett 2015;15(4):2756–62.
[40] Tan Z, Zhang W, Zhang Z, Qian D, Huang Y, Hou J, et al. High-performance inverted polymer solar cells with solution-processed titanium chelate as electron-collecting layer on ITO electrode. Adv Mater 2012;24(11):1476–81.
[41] Yang L, Xu B, Bi D, Tian H, Boschloo G, Sun L, et al. Initial light soaking treatment enables hole transport material to outperform spiro-OMeTAD in solid-state dye-sensitized solar cells. J Am Chem Soc 2013;135(19):7378–85.
[42] Bi C, Wang Q, Shao Y, Yuan Y, Xiao Z, Huang J. Non-wetting surface-driven high-aspect-ratio crystalline grain growth for efficient hybrid perovskite solar cells. Nat Commun 2015;6:7747.
[43] Gonzalez-Carrero S, Galian RE, Pérez-Prieto J. Maximizing the emissive properties of $CH_3NH_3PbBr_3$ perovskite nanoparticles. J Mater. Chem A 2015;3(17):9187–93.